UNIVERSITÀ DEGLI STUDI DI TRIESTE

DISPENSE DEL CORSO DI

FISICA DEGLI ACCELERATORI

DIAGNOSTICA:

CURRENT MONITOR

BEAM POSITION MONITORS

RF DEFLECTORS

ANNO ACCADEMICO 2012-2013

Contents

Chapter 1

The current monitor

The current monitor are diagnostic devices able to measure the beam current.

An electron beam is characterized by an electron charge Q, uniformly distributed in the space. We consider an electron beam travelling nearly at the speed of light 'c'. The longitudinal distribution ρ_z in the 'z' axis, so that:

$$Q = \int_0^l \rho_z(z)dz \tag{1.1}$$

we can also write:

$$Q = \int_0^{t_{end}} i(t)dt \tag{1.2}$$

where $i(t)$ is the instantaneous current. Fig. 1.1 shows an example of Gaussian current distribution.

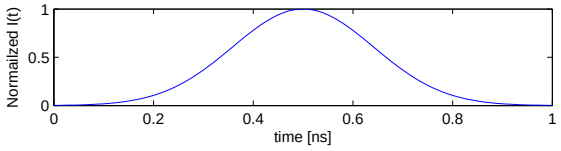

Figure 1.1: *Gaussian current distribution.*

we want to measure the total beam charge.

The magnetic field generated by the beam, at a distance 'r' is:

$$H_\phi(r) = \frac{i}{2\pi r} \tag{1.3}$$

We consider a toroid, where we have a coil that receives the generated magnetic field, as shown in Fig. 1.2.

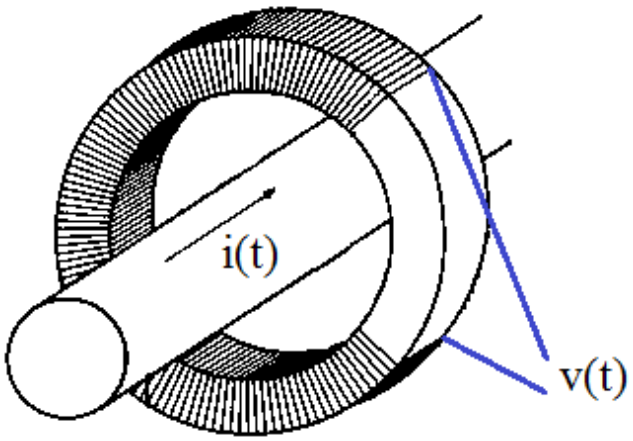

Figure 1.2: *Toroid crossed by an electron beam.*

From the Faraday-Lenz equation we have:

$$v(t) = N\frac{d\Phi}{dt} = N\frac{d}{dt}\frac{\mu i(t)A}{2\pi R} = \frac{N\mu A}{2\pi R}\frac{di(t)}{dt} \tag{1.4}$$

where N are the number of windings of the coil, A is the toroid transversal surface, R is the distance between the beam and the toroid. An example of the toroid output signal is the following:

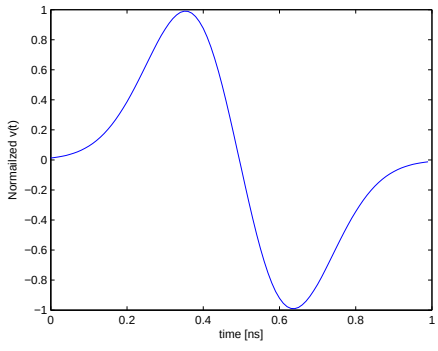

Figure 1.3: *Normalized toroid voltage.*

The beam current $i(t)$ can be determined with:

$$i(t) = \frac{2\pi R}{N\mu A} \int v(t)dt \tag{1.5}$$

and therefore the total beam charge with Eq. (1.2).

Chapter 2

The beam position monitors

2.1 Overview of the beam position monitor devices

The beam position monitor devices (BPMs) are used to determine the transversal position of the electron beam in vacuum beampipe. One of the main challenges in the synchrotrons and in the free electron lasers community is to determine such position with high accuracy.

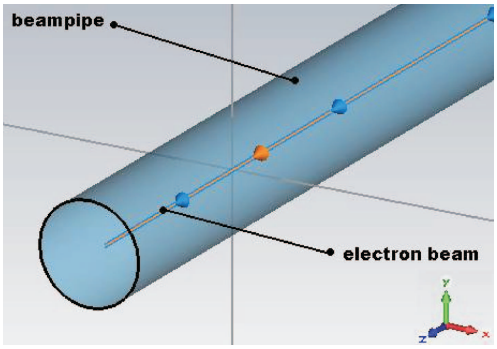

Figure 2.1: *Beampipe with electron beam.*

There are several kinds of devices used for this purpose. They are based on the wakefield generated by the transit of a ultra-relativistic electron beam [9]. In fact, an electron bunch travelling at high speed (usually with v $\approx$ c), generates an electromagnetic field (Fig. 2.2).

The generated wakefield is then used to determine the position of the electron beam, by determining its trace on a transversal plane XY (Fig. 2.3).

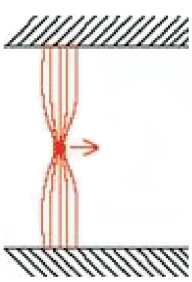

Figure 2.2: *Example of the wakefield generated by an electron beam.*

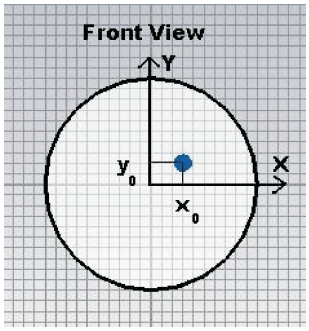

Figure 2.3: *X and Y position of the beam.*

2.2 Buttons BPMs

The buttons BPMs [10] [11] are made with four buttons placed in the beampipe, as shown in Fig. 2.4.

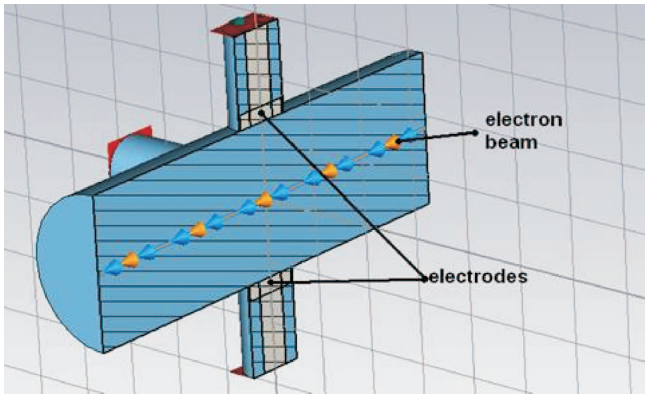

Figure 2.4: *Button BPM.*

The four buttons are electrodes that receive the beam wakefield. The

closer is the distance between the beam and one electrode, the higher is the signal collected by the respective electrode. It is possible to estimate the position of the bunch by elaborating the amplitude of the four signals.

The advantages of the button BPM are:

- they are easy to build;
- they do not affect the electron beam, because the geometry of the vacuum chamber is unchanged.

The disadvantages are:

- they have low output signal in singe bunch;
- they have low resolution in singe bunch.

Due to the low resolution in single bunch operation, they cannot be used in a single-pass free electron laser, because such FEL device operates with a single electron bunch, with low repetition rate. However, these devices are well employed in synchrotrons, because the same electron bunch crosses the BPM several times per second (due to the circular path of the electrons). In this way the output signal is emphasized. Moreover all the techniques of average and noise reduction can be applied.

An example of button BPM is reported as follows:

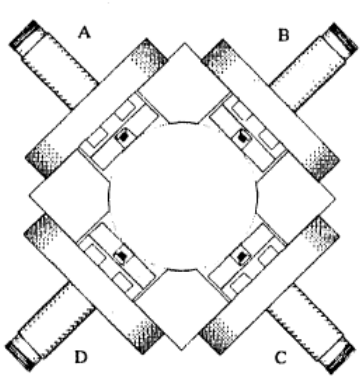

Figure 2.5: *Button BPM with 4 pickups.*

The horizontal position is determined with the following relation:

$$x = k_x \cdot \frac{(V_b + V_c) - (V_a + V_d)}{(V_a + V_b + V_c + V_d)} \tag{2.1}$$

while the vertical is:

$$y = k_y \cdot \frac{(V_a + V_b) - (V_c + V_d)}{(V_a + V_b + V_c + V_d)} \tag{2.2}$$

k_x and k_y are constants. They are determined during the calibration process.

Another type of button BPM is reported in Fig. 2.6.

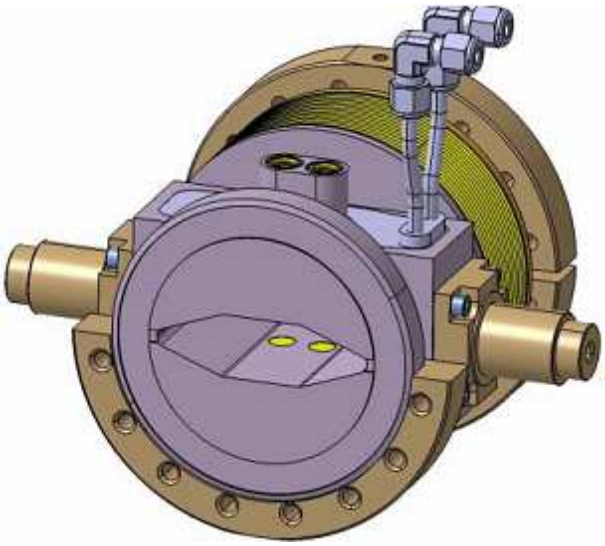

Figure 2.6: *Button BPM.*

2.3 Microstrip BPMs

The microstrip BPMs [12] [13] are made with four microstrip lines located inside the beampipe, as shown in Fig. 2.7.

The four microstrip lines resonate when the electron bunch crosses the BPM. The closer is the distance between the beam and one of the microstrips, the higher is the output signal collected from such microstrip. Elaborating the amplitude of the four collected signals, it is possible to estimate the

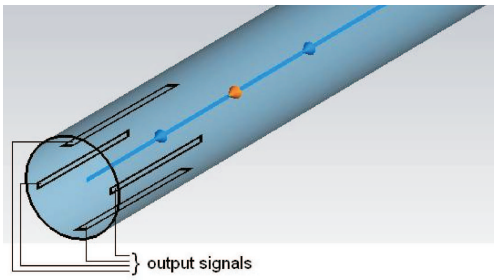

Figure 2.7: *Microstrip BPM.*

position of the bunch. This kind of devices can reach a resolution of 10 μm in single shot.

The electrodes are depicted in Fig. 2.8.

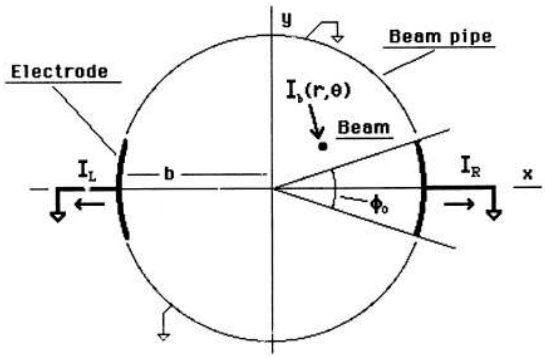

Figure 2.8: *Microstrip BPM electrodes.*

The aim in the stripline design is to obtain a device able to be sensitive to small beam variations. A high signal/noise ratio (SNR) is desired. Therefore the angle ϕ_0 of Fig. 2.8 determines the level of the output signal. A high value of ϕ_0 (up to 45 degrees) gives a high output signal. However, a high value of ϕ_0, makes the stripline insensible of small beam variations. In the stripline design the ϕ_0 value is a trade-off between the output signal level and the sensibility of small beam variations. A typical stripline BPM is reported in Fig. 2.9.

There are two types of stripline BPMs:

- The non resonant striplines;
- The resonant striplines.

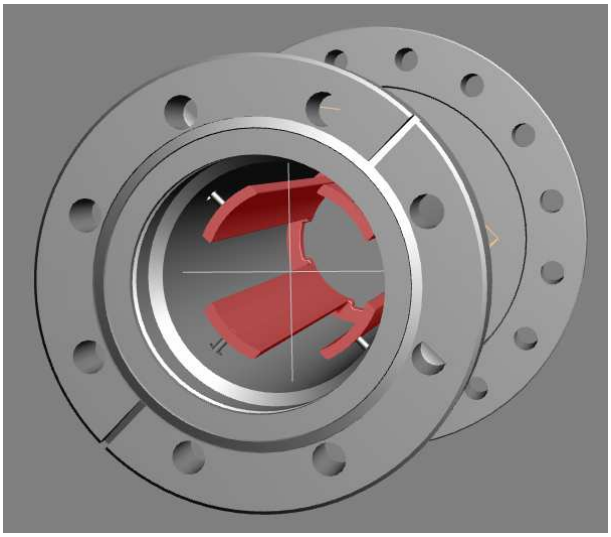

Figure 2.9: *Stripline BPM.*

In the first case, the stripline simply collects the beam wake fields. The typical output signal is reported in Fig. 2.10.

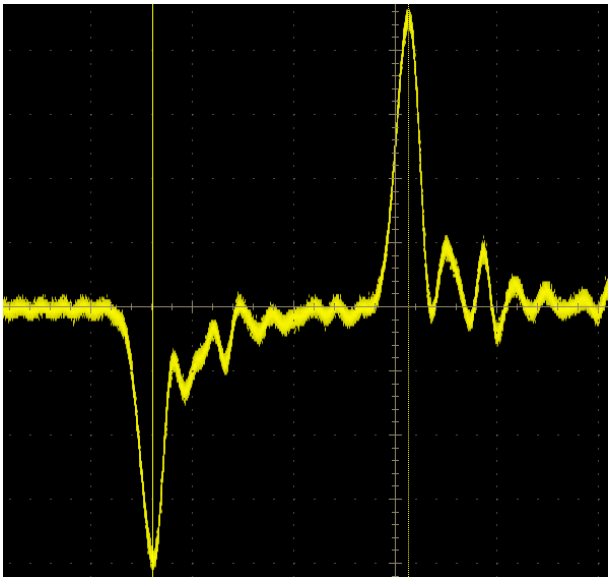

Figure 2.10: *Output signal from a non-resonant stripline.*

The first peak is the peak generated by the beam. The second peak is the reflected signal, because additional power is reflected by the termination of the stripline (usually the stripline is terminated on a short-circuit).

In the second case, the stripline can be modeled with a resonant RLC circuit. When the beam passes trough it, its electrodes resonates at the resonant frequency of the striplines. The typical output signal is reported in Fig. 2.11.

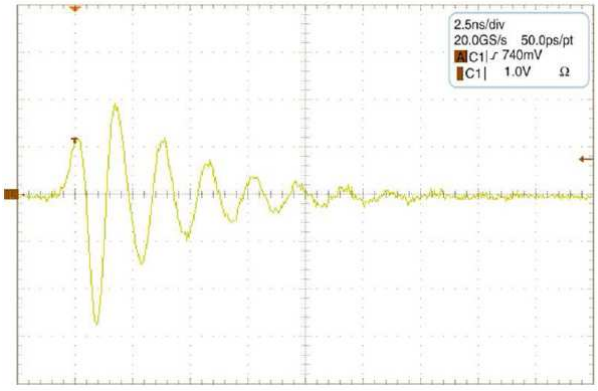

Figure 2.11: *Output signal from a resonant stripline.*

A problem of the microstrip BPM is that they have a small linear range. Alternative solutions can be employed to extend the linear range. Fig. 2.12 shows a different electrode that has a wider linear range (in the non-resonant case). The pickup of this picture, it is sensible to the vertical beam offset (another one is needed for the horizontal offset).

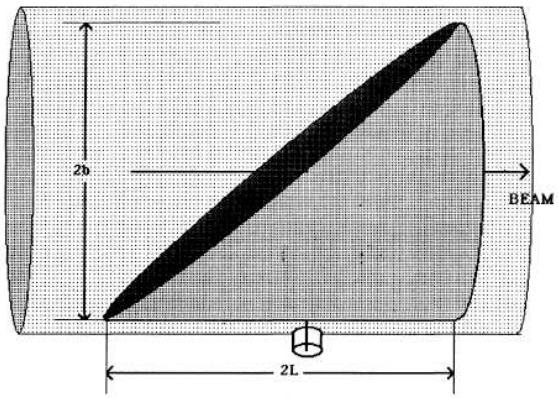

Figure 2.12: *Microstrip BPM electrode, with a wider linear range.*

2.4 The Cavity BPM

In order to obtain higher resolutions, in single shot, the cavity BPM has been used. It mainly consists of a resonant cavity and of some waveguides. The resonant cavity is located along the beampipe, as shown in Fig. 2.13.

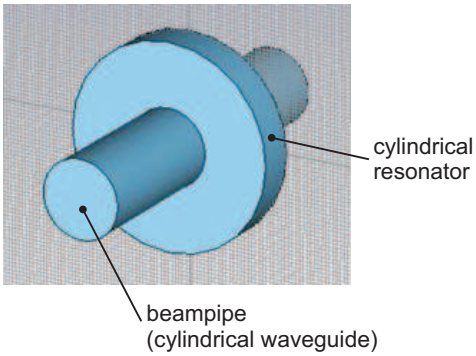

Figure 2.13: *Beampipe with resonant cavity.*

The electron beam can be modeled as a current distribution. When it passes through the cavity, it excites its resonant modes (Fig. 2.14).

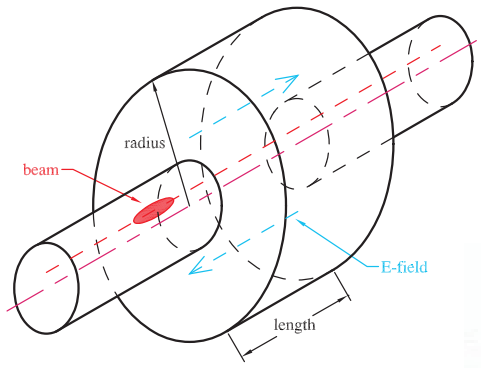

Figure 2.14: *Electron beam crossing the cavity.*

The first four modes in this type of cavity are:

- TM_{010}, also called "monopole";
- TM_{110}, also called "dipole";
- TM_{210}, also called "quadrupole";

- TM_{020}, also called "second monopole".

The electric field magnitude of such modes (simulated with Ansoft HFSS [3]), is depicted as follows:

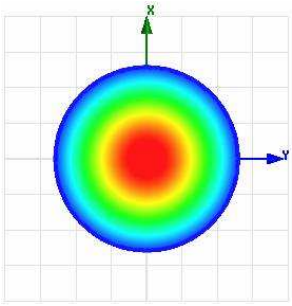

TM_{010}

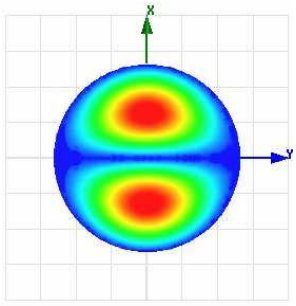

TM_{110}

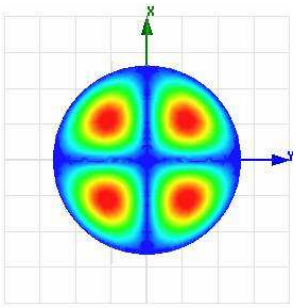

TM_{210}

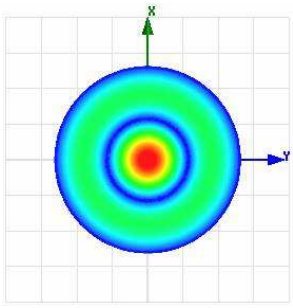

TM_{020}

The first two modes are the most relevant ones in this kind of device, and they must be considered when the cavity is used as beam position monitor. The signal of the resonant modes must be collected. Four rectangular waveguides are coupled with the resonant cavity and receive the signal (Fig. 2.15).

The four signals will be elaborated by the electronic devices described below, which will give the position of the electron beam. The resolution achieved by this kind of device is nearly 1 μm.

2.4.1 The dipole mode

The TM_{110} (dipole mode) is the most important mode of the cavity, and all the working operation of the BPM is related to it. In fact, the intensity of the dipole mode is proportional to the offset of the electron beam from the center axis of the beampipe (in the linearity range). There are two orthogonal polarizations: one is excited when the electron beam has a 'X' offset, the

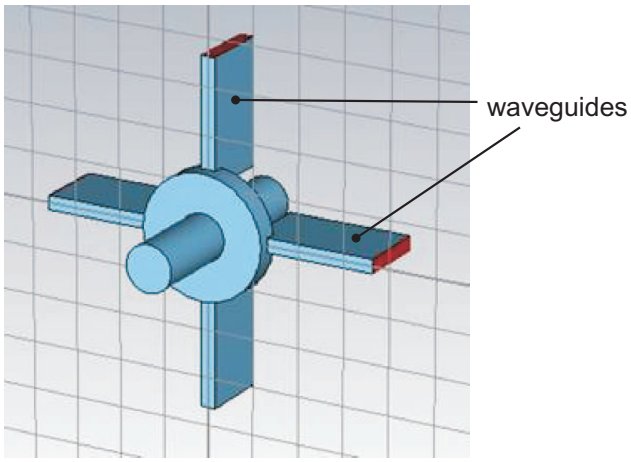

Figure 2.15: *Cavity BPM with the waveguides.*

other when the electron beam has an 'Y' offset. The E-field configuration of the two dipole polarizations is shown in Fig. 2.16.

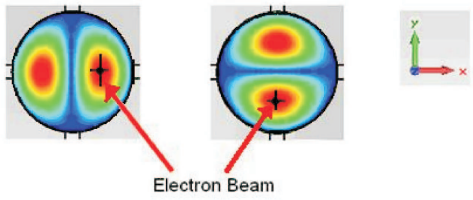

Figure 2.16: *Dipole X(horizontal) and Y(vertical) polarization of the E-field.*

The signals of the two polarizations (horizontal and vertical) must be separated in order to have one signal for the 'X' displacement and one for the 'Y' displacement. The separation is achieved with the cavity-waveguide coupling, where details are explained later on. The frequency target for the dipole is 6.5 GHz; hence the cavity will be designed and simulated to determine a particular radius that will satisfy such specifications.

2.4.2 The monopole mode

The TM_{010} mode (monopole) is an unwanted mode in the cavity BPM, because its signal voltage is only proportional to the beam intensity and does not depend on the beam position. The magnitude electric field configuration of the monopole is shown in Fig. 2.17.

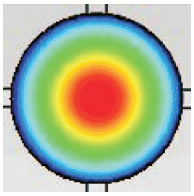

Figure 2.17: *Monopole electric field.*

The BPM is designed with a dipole resonant frequency of 6.5 GHz, and the monopole resonates at 4.6 GHz. Since the beam travels near the axis of the beampipe, the output signal of the monopole is very strong, while the dipole signal is very weak. Fig. 2.18 gives an example of such inequality.

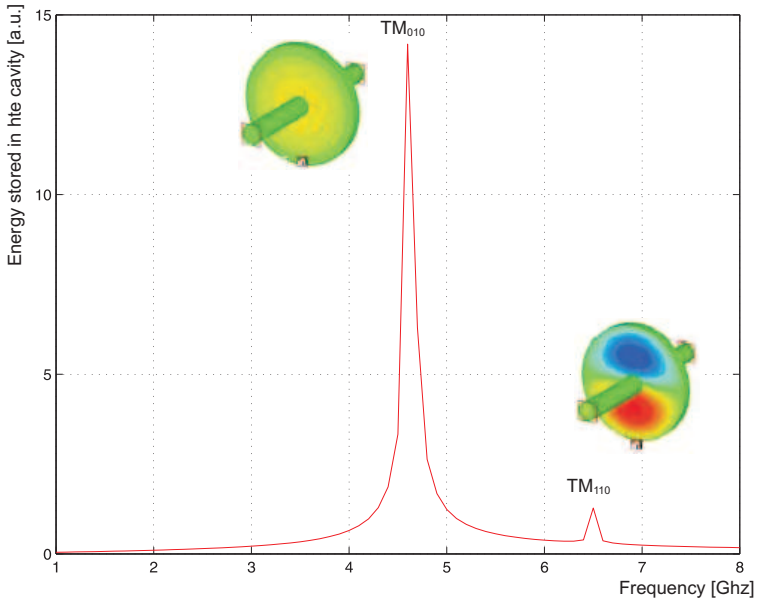

Figure 2.18: *Intensity of the modes arising in the cavity.*

In order to separate the TM_{010} from the TM_{110} signal, a band-pass filter centered at the dipole frequency (6.5 GHz) can be used. Additional solutions can be exploited for this purpose, in the electromagnetic design of the cavity, through the following expedients:

- Using the high-pass behavior of the rectangular waveguide;
- Using the magnetic coupling in the cavity-waveguide transition.

2.4.3 Rejection of the monopole mode with the waveguide cut-off frequency

The unwanted TM_{010} mode covers the weak signal of the position-sensitive TM_{110} mode. The first way to reject the monopole mode is the use of the cut-off frequency of the four rectangular waveguides. In fact, they behave as a high-pass filter, and the cut-off frequency for the dominant mode (TE_{10}) is given by:

$$f_L = \frac{c}{2a} \tag{2.3}$$

where c is the speed of light in the vacuum, and a is the maximum transversal dimension of the waveguide (Fig. 2.19). According to (2.3) the cut-off

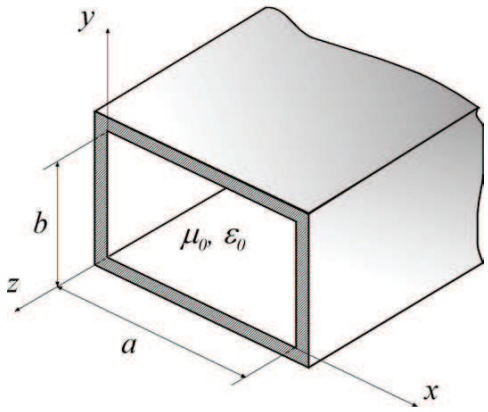

Figure 2.19: *Waveguide used to collect the cavity signals: a = 30 mm; b = 6 mm.*

frequency is 5 GHz, so the unwanted TM_{010} at 4.6 GHz is rejected.

2.4.4 Rejection of the monopole and separation of the two dipole polarizations with the magnetic coupling

The second way for rejecting the monopole exploites the cavity-waveguide coupler. This is called "magnetic coupler" [14], [15], because only the magnetic field of the dipole (TM_{110}) will couple with the waveguide. To analyze this kind of monopole rejection, let us study the field configurations in the cylindrical cavity resonator. The fields of the TM_{010} mode are given by:

$$E_z = CJ_0\left(\frac{j_{10}r}{R}\right)$$
$$H_\phi = -iC\frac{\omega\varepsilon_0 R}{j_{10}}J_0'\left(\frac{j_{10}r}{R}\right) \tag{2.4}$$

while the expressions for the TM_{110} mode are:

$$E_z = CJ_1\left(\frac{j_{11}r}{R}\right)\cos(\phi)$$
$$H_r = -iC\frac{\omega\varepsilon_0 R^2}{j_{11}^2}\frac{J_1\left(\frac{j_{11}r}{R}\right)}{r}\sin(\phi) \tag{2.5}$$
$$H_\phi = -iC\frac{\omega\varepsilon_0 R}{j_{11}}J_1'\left(\frac{j_{11}r}{R}\right)\cos(\phi)$$

where $j_{10} = 2.4$, $j_{11} = 3.83$, J_0 and J_1 are the Bessel functions of the first kind and order zero and one, respectively, R the cavity radius, r the radial position, ϕ the azimuth angle of a cylindrical coordinate system where z-axis coincides with the axis of the cavity, and C is a constant. These equations are a good approximation of the field configuration of the cylindrical resonator located along the beampipe. The dipole magnetic field lines, for an 'X' displacement of the electron beam, are reported in Fig. 2.20. In order to describe

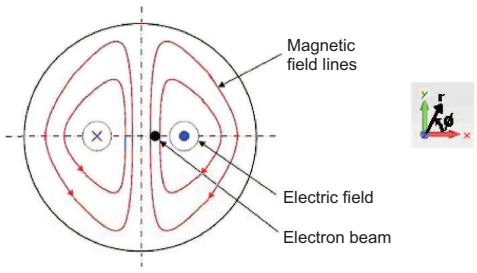

Figure 2.20: *Dipole magnetic field lines*

the magnetic coupling, Fig. 2.21 shows one coupler placed at ϕ=90^o. It is important to see (Fig. 2.21) that only H_r has the same direction as the H field of the waveguide, in the coupling volume cavity-waveguide. Therefore, a resonant mode in the cavity can generate the TE_{10} mode in the waveguide only if the resonant mode has a radial (H_r) component in proximity of the waveguide. Therefore the coupling is called "magnetic coupling" [14], [15],

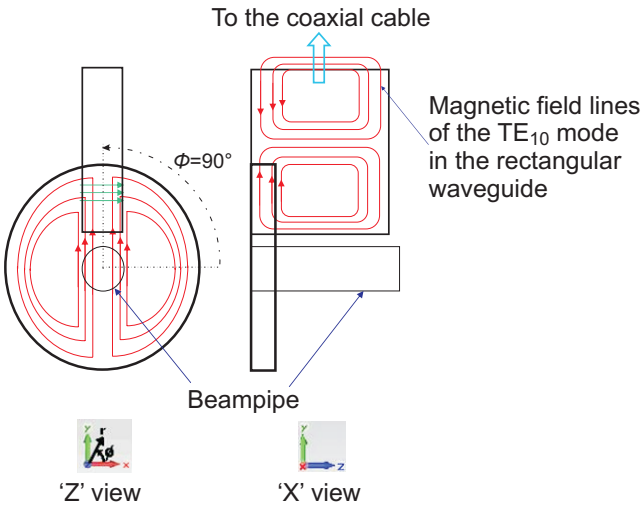

Figure 2.21: *Magnetic coupling.*

where H_r (in the cavity) couples with H in the waveguide. There are three important issues to analyze:

1. Effect of the monopole mode;
2. Effect of the dipole mode generated by an 'X' beam displacement;
3. Effect of the dipole mode generated by a 'Y' beam displacement.

The first case considers the effect of the monopole, which is always present for any displacement of the beam, and has a high intensity. However, it has only the H_ϕ component, but not the H_r component. Therefore, the magnetic coupling that works with H_r, will not transfer energy to the rectangular waveguides, as shown in Fig. 2.22.

In the second case the electron beam has an 'X' offset, and the dipole mode is oriented in the horizontal polarization. The magnetic coupling transfers energy only to the two vertical waveguides; therefore only port 1 and 3 will have an output signal, as shown in Fig. 2.23.

In the third case the electron beam has a 'Y' offset, and the dipole mode is oriented in the vertical polarization. The magnetic coupling transfers energy only to the two horizontal waveguides; therefore only ports 2 and 4 will have an output signal.

The magnetic coupling has the following advantages:

- It rejects the monopole mode

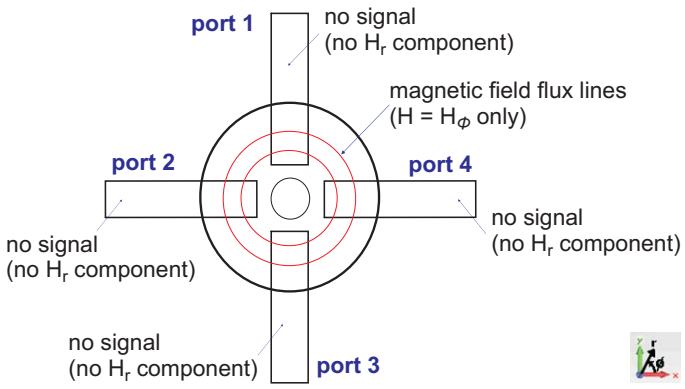

Figure 2.22: *Magnetic coupling with monopole.*

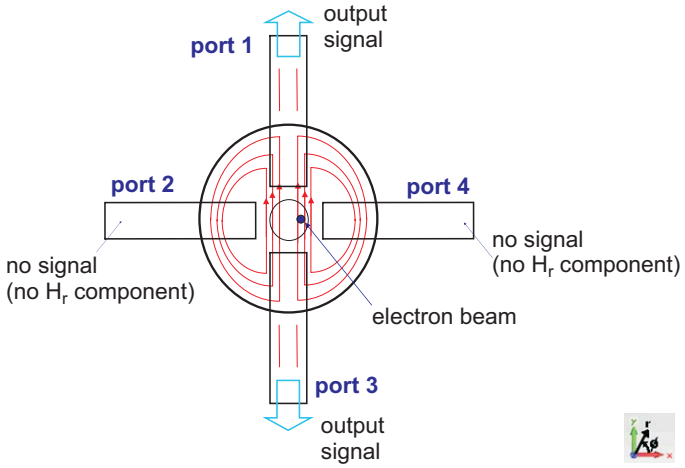

Figure 2.23: *Magnetic coupling with 'X' dipole.*

- It separates the horizontal polarization (whose signal exits only through ports 1 and 3) from the vertical one (whose signal exits only through ports 2 and 4).

2.4.5 The reference cavity

With reference to Fig. 2.23, the magnitude of the output signal of ports 1 and 3 is proportional to the absolute value of the X position, while the magnitude of the output signal of ports 2 and 4 is proportional to the absolute value of the Y position. When the beam trajectory passes from a positive offset (e.g., X = 0.1 *mm*), to a negative offset (e.g. X = -0.1 *mm*), the phase has a 180° change when the beam is passing through the zero position. In order to

measure both the positive and the negative beam offset, this phase inversion must be detected. To this purpose, an additional reference cavity is needed. The reference cavity works with a monopole mode at 6.5 GHz. Such signal is independent of the beam position. An example of the signal generated by the reference cavity, and of the signal generated by the position cavity, with both a negative and a positive beam offset, is illustrated in Fig. 2.24. The electronic system receives three signals: those related to the X and Y

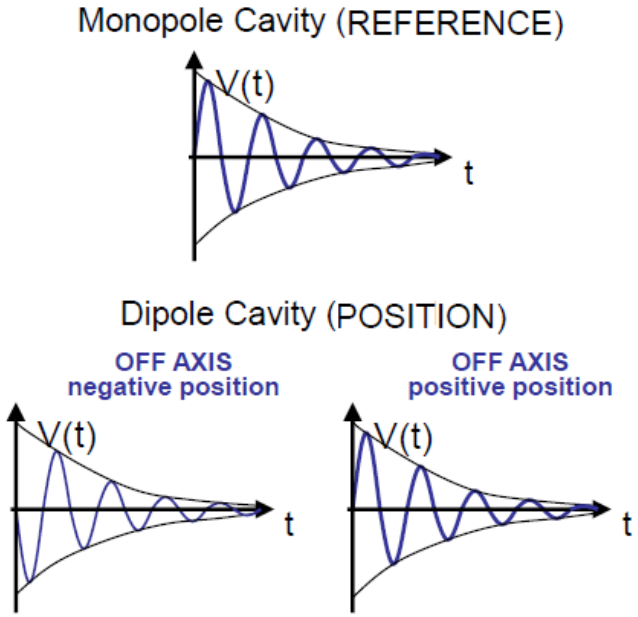

Figure 2.24: *Output signals from the reference and the position cavities.*

position, and the reference signal, as depicted in Fig. 2.25. With the reference signal, the electronic system is able to recognize positive and negative beam offsets. The traditional way to achieve such purpose, is based on the use of the IQ (In-phase, in-quadrature) demodulation [16] [17].

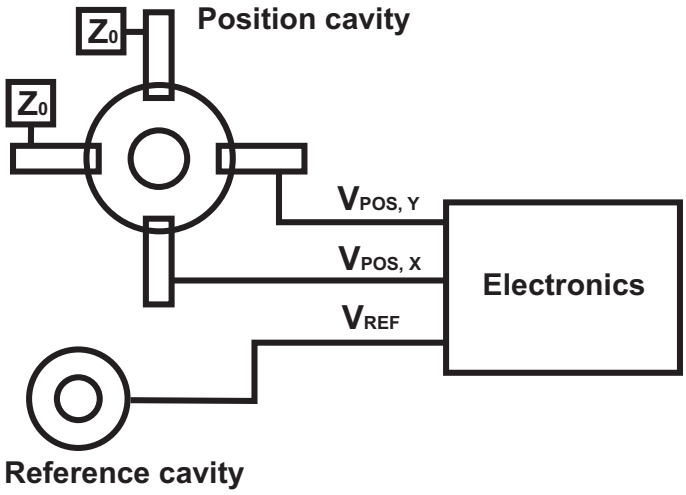

Figure 2.25: *Cavities and electronic system.*

Chapter 3

The RF deflectors

3.1 Resonant modes in a cylindrical pillbox

Let us consider a cylindrical pillbox, as shown in Fig. 3.1.

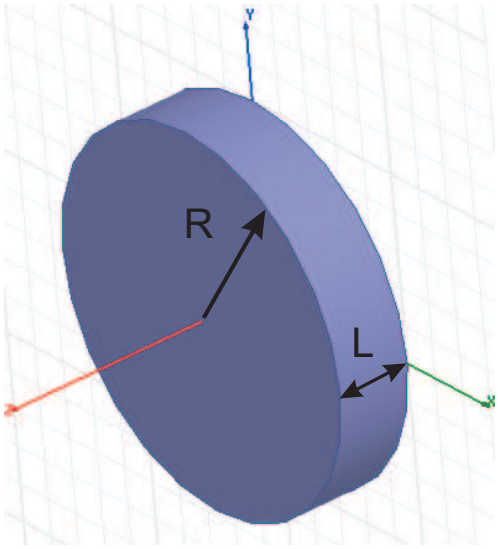

Figure 3.1: *Cylindrical pillbox.*

If the cavity L/R ratio is lower than 2.03, the first resonant mode is the TM_{010}. From the electromagnetic theory, the resonant frequency of the monopole is given by:

$$f_{TM010} = \frac{c}{2\pi}\frac{j_{01}}{R} \tag{3.1}$$

where $j_{10} = 2.4$. The second TM resonant mode is the dipole mode TM_{110}. Its resonant frequency is given by:

$$f_{TM110} = \frac{c}{2\pi}\frac{j_{11}}{R} \tag{3.2}$$

where $j_{11} = 3.83$. The fields of the TM_{010} mode are given by:

$$\begin{aligned} E_z &= CJ_0\left(\tfrac{j_{10}r}{R}\right) \\ H_\phi &= -iC\tfrac{\omega\varepsilon_0 R}{j_{10}}J_0'\left(\tfrac{j_{10}r}{R}\right) \end{aligned} \tag{3.3}$$

while the expressions for the TM_{110} mode are:

$$\begin{aligned} E_z &= CJ_1\left(\tfrac{j_{11}r}{R}\right)\cos(\phi) \\ H_r &= -iC\tfrac{\omega\varepsilon_0 R^2}{j_{11}^2}\tfrac{J_1\left(\frac{j_{11}r}{R}\right)}{r}\sin(\phi) \\ H_\phi &= -iC\tfrac{\omega\varepsilon_0 R}{j_{11}}J_1'\left(\tfrac{j_{11}r}{R}\right)\cos(\phi) \end{aligned} \tag{3.4}$$

where J_0 and J_1 are the Bessel functions of the first kind and order zero and one, respectively, R the cavity radius, r the radial position, ϕ the azimuth angle of a cylindrical coordinate system where z-axis coincides with the axis of the cavity, and C is a constant.

The electric field magnitude of such modes (simulated with Ansoft HFSS [3]), is depicted as follows:

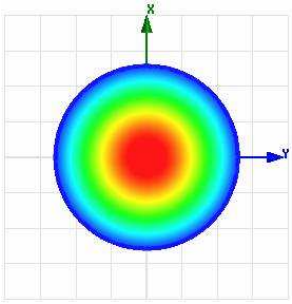

TM_{010}

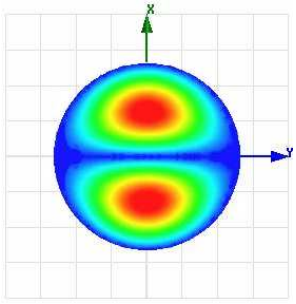

TM_{110}

3.2 The RF linear accelerators

The RF linear accelerators are composed of a series of resonant cavities, working with the TM_{010}, which is the accelerating mode. An example of

linear accelerator is depicted in Fig. 3.2, 3.3. The RF power arrives with a waveguide and it is couped with the series of pillboxes.

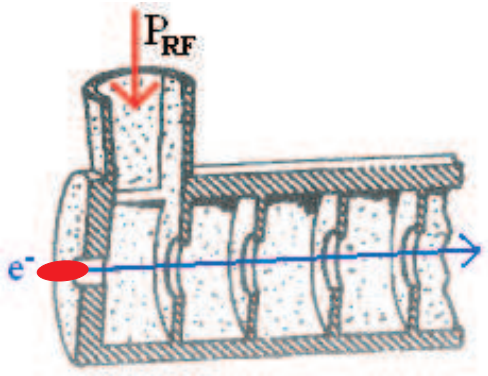

Figure 3.2: *Beam acceleration.*

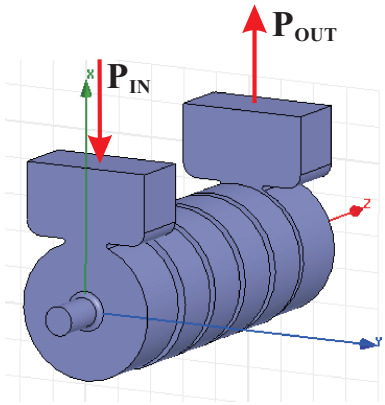

Figure 3.3: *Single feed travelling wave accelerating structure.*

According to Eq. (3.3), the electric field is oriented along the 'z' direction, therefore the electrons receive a longitudinal force.

3.3 The RF deflectors

The RF deflectors are travelling wave disk loaded structures in which an electromagnetic field can interact with ultra-relativistic electron bunches, providing a constant transversal force [26]. The deflection is generated by the TM_{110}, the dipole mode. When the deflector is turned on, the electron

bunch is stretched by a transversal deflecting voltage and is forced to collide with a detector screen, as illustrated in Fig. 3.4 3.5, thus recording the beam longitudinal profile. The beam trace on the screen is then converted into an optical signal to be processed. When the deflector is turned off, the detector screen is removed and the beam simply passes through the device without being deflected, and is used to produce a free electron laser (FEL) radiation.

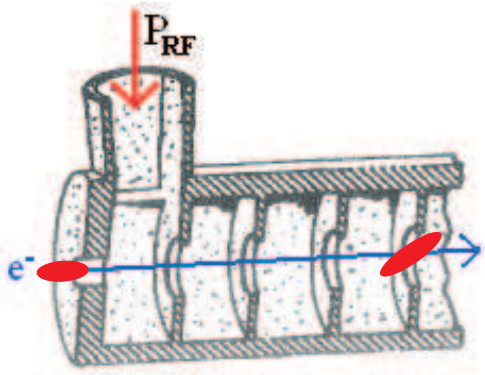

Figure 3.4: *Beam deflection.*

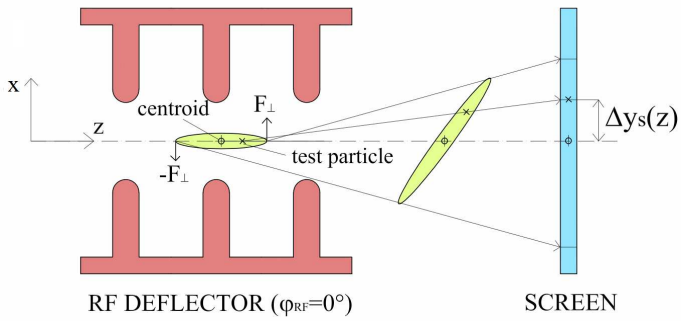

Figure 3.5: *RF beam deflection.*

The deflection is generated by the TM_{110}, the dipole mode. Eq. (3.4) shows that the electric field, when present, is oriented along the 'z' direction. Therefore it cannot deflect the beam. The deflection is generated by the magnetic field.

The effective energy exchange is described by the Panofsky-Wenzel theorem [24].

3.3.1 The Panofsky-Wenzel theorem

The Panofsky-Wenzel theorem [24] shows that the electron beam receives a transversal kick as well. Precisely, the transversal momentum ($p_\perp$) is given by:

$$p_\perp = j\frac{q}{\omega}\int_0^l \nabla_\perp E_z dz \tag{3.5}$$

where q is the electron charge, ω the angular frequency, and l the coupler length.

Here we will propose a simple justification of the Panofsky-Wenzel theorem. According to Eq. 3.4, in an ideal pillbox working with the TM_{110} mode, the electric field is only longitudinal, therefore $\overrightarrow{E} = E_z \overrightarrow{k}$.

The electron beam is travelling through the 'z' axis, at the speed of light 'c'.

Therefore the transversal force is generated by the magnetic field H_y (in the proximity of the axis we consider $\overrightarrow{H} \approx H_y \overrightarrow{j}$).

The transversal Lorentz force is therefore:

$$F_x = -qcB_y \tag{3.6}$$

while the momentum is:

$$p_x = \int_0^{t_{end}} F_x dt = \frac{1}{c}\int_0^l F_x dz = -q\int_0^l B_y dz \tag{3.7}$$

From the Maxwell equation, $\overrightarrow{B} = j\overrightarrow{\nabla} \times \overrightarrow{E}/\omega$. Calculating B_y from the Maxwell equation, and substituting it in 3.7, we obtain:

$$p_x = -q\int_0^l (-\frac{j}{\omega}\frac{\partial E_z}{\partial x})dz. \tag{3.8}$$

Therefore:

$$p_x = j\frac{q}{\omega}\int_0^l \frac{\partial E_z}{\partial x}dz. \tag{3.9}$$

With this relation is possible to estimate the beam deflection from the electric field.

3.4 Effect of the RF phase

The electron beam is travelling at the speed 'c', synchronous with the phase velocity of the deflecting mode. For a single particle we can write:

$$z = z_0 + ct \tag{3.10}$$

For the deflecting mode we can write:

$$B_y(z,t) = B_{yPEAK} \cdot sin(\Phi_{RF} + \omega t - kz) \tag{3.11}$$

Supposing $z_0 = 0$, and the synchronism between the particle and the electromagnetic field, $\omega t - kz = 0$. The transversal force depends on the relative position between the electron and the RF phase. In particular, for a single particle:

$$F_x = F_{xPEAK} \cdot sin(\Phi_{RF}) \tag{3.12}$$

A long electron bunch is composed by multiple particles. Each one of them is at a different RF phase. We must modify the above equation, introducing the variable ζ [m], that is the relative position of every single particle, with respect to the center, obtaining:

$$F_x = F_{xPEAK} \cdot sin(\Phi_{RF} - k\zeta) \tag{3.13}$$

This equation shows that the electrons located at different longitudinal positions receive different transversal forces. Fig. 3.6 shows the typical situation of the electron beam, during the deflection process.

This particular condition is called zero-crossing:

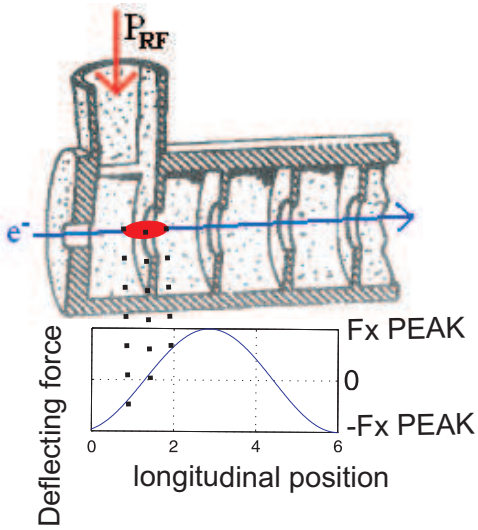

Figure 3.6: *Beam deflection at different RF phases.*

- The particle located in the beam center does not receive a transversal force;
- The head particle (the first particle of the beam) receives a positive transversal force;
- The tail particle (the last particle of the beam) receives a negative transversal force.

In the synchronism condition between the electrons and the phase velocity of the electromagnetic field, the beam is constantly stretched when crossing the cavity. Fig. 3.7 shows the typical situation of the electron beam, during the deflection process.

In this way every particle of the beam is stretched with a constant transversal force, and the next section will show such measurements.

3.5 Electron beam measurements

Radio-frequency deflectors are used to perform bunch length measurements and phase space diagnostics in the light source accelerators [27] [28]. These measurements are used to asses the quality of the electron beam, before entering in the undulator chains, at 1.2 GeV.

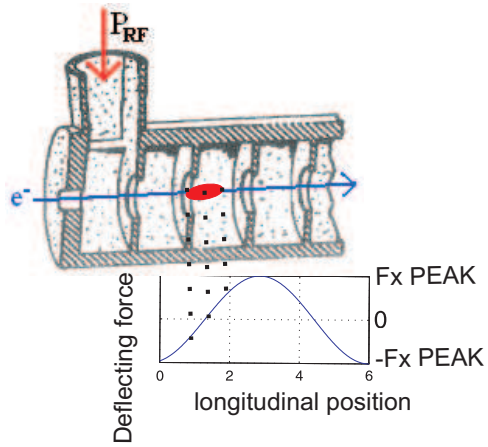

Figure 3.7: *Beam deflection in a following time instant.*

Two High Energy RF Deflectors (HERFD) have been realized for the FERMI@Elettra project. They have the aim of stretching the electron bunch horizontally and vertically, respectively. The two cavities are individually powered by the same klystron and a switch system is used to choose the deflection plane.

The specifications of the two HERFD are reported in Table 3.1.

Table 3.1: HERFD specifications.

Frequency (f)	2998.01 MHz
Deflecting voltage (V_t)	20 MV
Filling time (t_F)	500 ns
Input power (P_{in})	15 MW
Length	2.5 m

The electron bunch length has been measured with the two deflectors, at first by using the vertical deflector, and then by the horizontal one. The bunch length values have been compared. Fig. 3.8 shows the beam vertical deflection, while Fig. 3.9 shows the beam horizontal deflection.

The measured bunch lengths RMS values are 0.44 ps by using the vertical deflector, and 0.43 ps by using the horizontal deflector. These measurements are in good agreement. The deflectors are ready to be used in slice emittance and phase-space measurements.

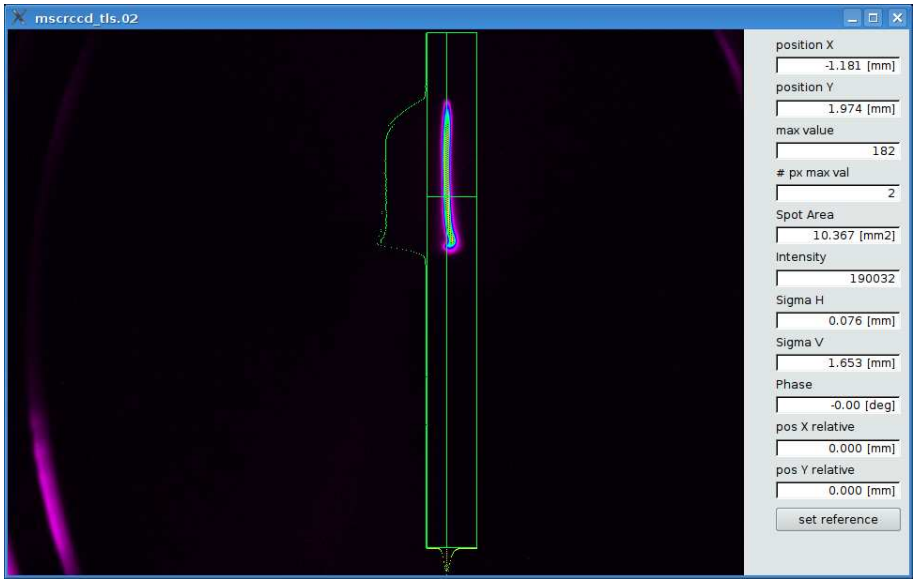

Figure 3.8: *Beam deflection in the vertical plane.*

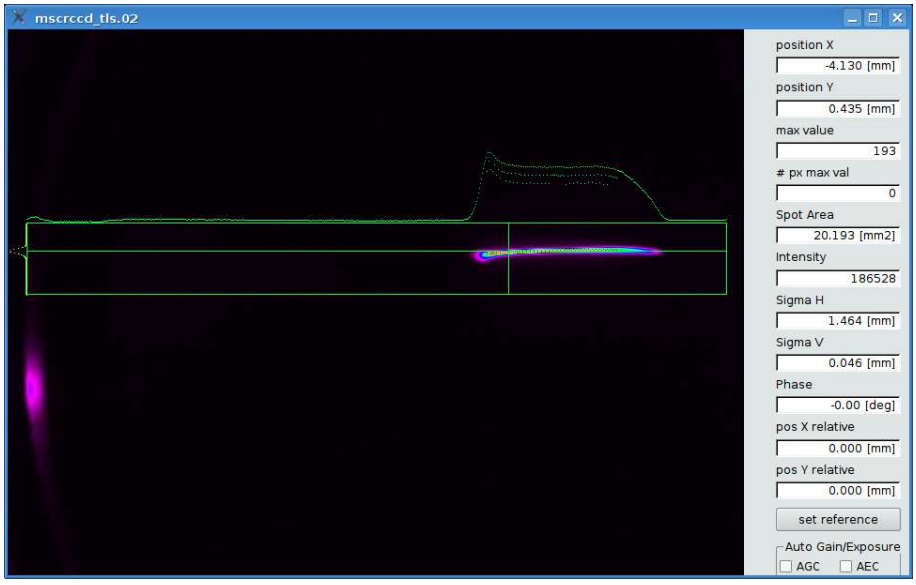

Figure 3.9: *Beam deflection in the horizontal plane.*

Bibliography

[1] E. Allaria et al., "Highly coherent and stable pulses from the FERMI seeded free-electron laser in the extreme ultraviolet", *Nature Photonics*, pp. 699-704, 2012.

[2] C. J. Bocchetta et al., "FERMI@Elettra Conceptual Design Report", Sincrotrone Trieste, Italy, Tech. Rep. ST/F-TN-07/12, 2007.

[3] HFSS, `http://www.ansoft.com/products/hf/hfss/`.

[4] CST, `http://www.cst.de/`.

[5] Z. Li et al., "Coupler design for the LCLS injector S-Band structures", Proceedings of PAC 05, Particle Accelerator conference, May 16-20, 2005, Knoxville, Tennessee, USA.

[6] E. L. Saldin et al., "The Physics of Free Electron Lasers", Springer, Berlin, 2000.

[7] J. D. Jackson, "Classical Electrodynamics", John Wiley & Sons, Inc., New York, 1999.

[8] H. Wiedemann, "Synchrotron Radiation", Springer, Berlin, 2003.

[9] A. W. Chao, "Physics of Collective Beam Instabilities in High Energy Accelerators", John Wiley & Sons, Inc., New York, 1993.

[10] J. Hinkson, "Advanced Light Source Beam Position Monitor", Accelerator Instrumentation Third Annual Workshop, Conference Proceedings n. 252, October 28-31, 1991, Newport News, VA, USA.

[11] P. Wang et al., "Beam position monitors for Duke FEL stroage ring", Proceedings of PAC 1999, Particle Accelerator Conference, March 29 - April 2, 1999, New York, USA.

[12] R. E. Schafer, "Beam Position Monitoring", AIP Conference Proceedings on Accelerator Instrumentation, Volume 212, October 23-26, 1989, Upton, NY, USA.

[13] P. Evtushenko et. al., "Stripline beam position monitors for ELBE", Proceedings DIPAC 2001, beam Diagnostics and Instrumentation for Particle Accelerators Conference, May 13-15, 2001, Grenoble, France.

[14] Balakin et al., "Experimental results from a microwave Cavity Beam Position Monitor", Proceedings of PAC 1999, Particle Accelerator conference, March 29 - April 2, 1999, New York, USA.

[15] Zenghai Li et al., "Cavity BPM with dipole-mode-selective coupler", Proceedings of PAC 2003, Particle Accelerator conference, May 12-16, 2003, Portland, Oregon, USA.

[16] S. Waltson et al., "Performance of a high resolution cavity beam position monitor system", Nuclear Instruments and Methods in Physics Research A, Volume 578, 2007, pp. 1-22.

[17] Y. Inoue et al., "Development of a high-resolution cavity-beam position monitor", Physical Review Special Topics - Accelerators and Beams 11, 062801, 2008.

[18] H. Padamsee et al., "RF Superconductivity for Accelerators", John Wiley & Sons, Inc., New York, 2008.

[19] J.C. Slater, "Microwave Electronics", Van Nostrand, Princeton, New York, 1950, Chap. 4, pp. 80-82.

[20] A. Marinelli, "Progetto di un accoppiatore in guida d'onda per una struttura accelerante ad onda viaggiante in banda X", X-band coupler for RF gun master thesis, University of Rome "La Sapienza", 2004.

[21] T. Wangler, "Introduction to linear accelerators", Los Alamos National Laboratory, 1994.

[22] P. M. Lapostolle, A. L. Septier "Linear Accelerators", North-Holland publishing company, Amsterdam, 1970.

[23] G. A. Loew et al., "The Stanford Two-Mile Accelerator", W. A. Benjamin, Inc, New York, pp. 146-148, 1968.

[24] W.K. H. Panofsky and W. Wenzel, "Some Consideration concerning the Transverse Deflection of Charged Particles in Radio-Frequency Fields", Rev. Sci. Instr., 27, pag. 967, 1956.

[25] G. A. Loewl et al., "Microwave measurements of azimuthal asymmetries in accelerating field of disk-loaded waveguides", IEEE Transaction on Nuclear Science, Vol NS-30, No. 4, August 1983.

[26] M. Petronio, "Research and Applications of Radio-Frequency Deflecting Cavities", PhD Thesis, University of Trieste, 2010.

[27] P. Emma et al., "A transverse RF deflecting structure for bunch length and phase diagnostic", Proceedings of PAC 01, Particle Accelerator conference, June 18-22, 2001, Chicago, Illinois, USA.

[28] G. A. Loew, "Design and application of RF separator structures at SLAC", PUB 135, Standford linear accelerator center, Standford University, California, August 1965.